Polar interactions determine head domain-mediated vinculin oligomerization induced by the *Shigella* IpaA effector

Benjamin COCOM-CHAN[1-3], Hamed KHAKZAD[1-3], Cesar VALENCIA-GALLARDO[1-3], Yosra ZARROUK[1-3], Guy TRAN VAN NHIEU[1-3*]

[1]Team "Ca^{2+} signaling and Microbial Infections", I2BC, 91190 Gif-sur-Yvette, France.

[2]Institut National de la Santé et de la Recherche Médicale U1280, 91190 Gif-sur-Yvette, France.

[3]Centre National de la Recherche Scientifique UMR9198, 91190 Gif-sur-Yvette, France.

[*] correspondance : guy.tranvannhieu@i2bc.paris-saclay.fr

Running title: IpaA-induced head domain-vinculin oligomerization

Keywords: ***vinculin; head domain; oligomerization; cell adhesion***

Abstract

Vinculin is a component of focal adhesions strengthening integrin receptors association to the actin cytoskeleton during mechanotransduction. While vinculin activation leading to its association with actin filaments has been particularly studied, the role and mechanism of vinculin oligomerization remain unclear. The *Shigella* IpaA effector binds to vinculin to promote efficient bacterial invasion of host cells. Unlike canonical activating ligand, IpaA interacts with the vinculin subdomains D1 and D2 via its three Vinculin Binding Sites (VBSs), promoting major allosteric changes leading to D1D2 domain-mediated trimerization. Here, we built on structural models of allosteric conformers of D1D2:IpaA complexes to design mutations and analyzed their effects on IpaA-induced trimer formation using native gel shift assays. We show that charge inversions, mutations affecting polar interactions at residues in D1D2 interfacing IpaA VBS3 and targeting a distal putative coiled-coil motif in D2 reduced the rates of D1D2 trimer formation. Introduction of these mutations in full-length vinculin led to a decrease in the number and size of focal adhesions, with distinct elongated focal adhesions associated with the coiled-coil mutation. These findings suggest that IpaA hijacks a cell endogenous head-domain mediated vinculin oligomerization process involved in the maturation of focal adhesion.

Introduction

Vinculin is a cytoskeletal linker of integrin-mediated matrix adhesions as well as cadherin-based cell-cell junctions (Goldman, 2016; Bays and De Mali, 2017). It plays an important role in cell adhesion processes, motility and development and its functional deficiency is associated with major diseases including cancer and cardiomyopathies (Peng et al., 2011). Vinculin associates with a number of ligands, including focal adhesion and intercellular junction components, lipids, signaling proteins as well as proteins regulating the organization and dynamics of the actin cytoskeleton (Goldman, 2016; Bays and De Mali, 2017). The role of vinculin in integrin-mediated adhesion has been particularly studied (Atherton et al., 2016; Parsons et al., 2010). Vinculin is recruited at focal adhesions and reinforces the link between integrins and the actin cytoskeleton. The extent of vinculin recruitment determines the growth and maturation of focal adhesions, associated with the scaffolding of adhesion components and mechanotransduction linked to the actomyosin contraction (Atherton et al., 2016; Parsons et al., 2010). While the precise mechanisms leading to vinculin activation involving combinatorial stimulation and recruitment at focal adhesions in cells are not fully understood, in vitro biomimetic mechanical and structure-function studies have enlightened major aspects of the role of vinculin in cell adhesion (Yan et al., 2015).

Vinculin is classically described as a three-domain protein containing an aminoterminal globular head domain (Vh), a flexible linker domain, and a F-actin -binding tail domain (Vt). Vh contains three subdomains D1-D3 and a small subdomain D4. With the exception of D4 containing a single helix bundle, each D1-D3 subdomain corresponds to a conserved repeat consisting of two four/five helix bundles connected by a long alpha-helix (Goldman, 2016). At the inactive state, vinculin is maintained folded by intramolecular interactions between Vh and Vt. All ligands activating vinculin contain a vinculin binding site (VBS), corresponding to 20-25 residues structured into an amphipathic α-helix that interacts with the first helix-bundle of D1 (Gingras et al., 2005). Insertion of the activating VBS in the D1 first helix bundle leads to the reorganization of the bundle and destabilizes the interaction between D1 and Vt (Izard et al., 2004). More than 70 VBSs or predicted VBSs have been identified in the various vinculin ligands, often containing multiple VBSs (Kluger et al., 2020). These VBSs, however, are often buried into helix bundles and their exposure regulates vinculin activation (Kluger et al., 2020). Force-induced stretching of a vinculin ligand such as talin, acting as mechanosensor, provides

with a means to expose the VBSs during integrin-mediated adhesion (Sun et al., 2016; Goult et al., 2021). Talin binds to F-actin via at least two sites in its rod domain and to integrin cytoplasmic domains via its amino-terminal FERM domain. During mechanotransduction, talin stretching by the actomyosin contraction exposes vinculin binding sites (VBSs) that are buried in helix bundles of the rod domain in the native state (Yan et al., 2015). Exposed talin VBSs in turn bind to vinculin and relieve the intramolecular interactions between the vinculin head (Vh) and tail (Vt) domains, unveiling the F-actin-binding site in Vt (Goult et al., 2021). Since talin contains 11 VBSs in helix bundles unfolding at different force amplitudes, the stretching force-dependent interaction between talin and vinculin serves as a mechanism to strengthen actin cytoskeletal anchorage as a function of substrate stiffness (Yan et al., 2015; Yao et al., 2016). In vitro, vinculin interaction with a VBS is sufficient to promote its opening and interaction with F-actin. Vinculin activation in cells, however, may result from a combinatorial stimulus including interaction with F-actin, phosphatidylinositol (4,5)-biphosphate (PIP2) or phosphorylation (Izard and Brown, 2016; Aurnheimer et al., 2015).

Intracellular bacterial pathogens such as *Chlamydia*, *Rickettsia*, and *Shigella* express ligands diverting vinculin functions to promote virulence (Thwaites et al., 2015; Park et al., 2011; Valencia-Gallardo, 2015). Among these, the *Shigella* type III effector IpaA was shown to target vinculin via three VBSs present at its carboxyterminal domain (Valencia-Gallardo, 2015). Unlike other host cell endogenous VBSs, IpaA VBSs are not buried into helix bundles and therefore likely act in concert to promote bacterial invasion. IpaA VBS1 and VBS2 bind to the first and second bundles of D1, respectively, conferring binding to vinculin with a very high affinity and the IpaA property to act a “super-mimic” of endogenous activating VBSs (Izard et al., 2006; Tran Van Nhieu and Izard, 2007). The role of IpaA VBS3 appears more complex and likely underline the role of IpaA in different processes during bacterial invasion. In addition to vinculin, IpaA VBS3 also binds to talin and may stabilize a partially stretched talin conformer present in filopodial adhesions, thereby favoring bacterial capture by filopodia at initial stages of the bacterial invasion process (Park et al., 2011; Valencia-Gallardo et al., 2019). IpaA VBS3 was also shown to bind to the vinculin D2 subdomain, when IpaA VBSs 1-2 are bound to D1 (Valencia-Gallardo et al., 2022). Binding of IpaA VBS1-3 to D1D2 trigger major conformational changes, coined “supra-activation”, leading to D1D2 homo-oligomerization via the D1D2 head subdomains and the formation of D1D2 trimers (Valencia-Gallardo et al., 2022). IpaA-induced

vinculin “supra-activation” enables invasive Shigella to promote strong adhesion in the absence of mechanotransduction (Valencia-Gallardo et al., 2022). However, analysis of defects a vinculin cysteine-clamp variant, deficient for vinculin supra-activation while still proficient for canonical activation, suggests that vinculin head domain oligomerization also occurs during mechanotransduction and is required for vinculin-dependent actin bundling and the maturation of focal adhesions into large adhesion structures (Valencia-Gallardo et al., 2022).

Seminal studies based on rotary shadow electron microscopy analysis reported the formation of vinculin mediated by Vh-Vh as well as Vt-Vt interactions in vitro(Molony and Burridge, 1985). Ever since, studies on vinculin oligomerization have essentially focused on Vt-Vt interactions. Phosphatidylinositol (4, 5) bisphosphate (PIP2) binding to vinculin was shown to promote vinculin oligomerization and PIP2-binding deficient vinculin showed defects in the organization of the actin cytoskeleton, as well as increased turn-over of focal adhesions (Bakolitsa et al., 1999; Chinthalapudi et al., 2014). Binding of F-actin was also reported to induced the formation of vinculin tail dimers, likely different than those induced by PIP2, and mutants in the Vt C-terminal hairpin responsible for F-actin-induced dimerization showed defects in actin bundling associated with a decrease in size and number of focal adhesions (Johnson and Craig, 2000; Bakolitsa et al., 1999). Vinculin establishes catch bonds with a significantly increased lifetime when the force is applied towards the pointed end of actin filaments, consistent with the polarity of actomyosin contraction (Huang et al., 2017). However, while mechanotransduction triggers vinculin recruitment associated with the maturation, enlarging of focal adhesions and actin bundling, how Vt-mediated vinculin oligomerization may be regulated by actomyosin contraction remains unclear (Thompson et al., 2013). Vinculin head-domain (Vh) mediated oligomerization could provide with a force-dependent mechanism, since vinculin was reported to acts as a mechanosensor, with its head domain undergoing conformational changes under applied force, showing increased binding to ligand such as MAPK1 (Garakni et al., 2017). Here, we report the effects of mutation in vinculin D1D2 altering the formation of trimers induced by IpaA. We identified D1D2 polar residues predicted to contact IpaA VBS3 and showed their involvement in IpaA-induced trimerization. We show that these mutations affect the formation of focal adhesions

supporting the notion that Vh-Vh mediated vinculin oligomerization akin to that induced by *Shigella* IpaA also occurs during the maturation of cell adhesion structures.

Results

Design of mutations in D1D2 affecting IpaA-induced trimer formation

The modeled structures indicated that the IpaA VBS3 interacted with D2 and triggers a reorganization of the D1 and D2, where the major axis of these subdomains underdoes a 30 % angle displacement relative to the apo D1D2 or D1D2 in complex with IpaAVBS1-2 only (Fig. 1B, Valencia-Gallardo et al., 2022). This "open" D1D2 conformer is associated with D1D2-mediated trimerization of vinculin (Valencia-Gallardo et al., 2022), since IpaA VBS1-2 was found to form D1D2:IpaA 1:1 and 2:0-2:1 complexes, while IpaA VBS1-3 also triggered the formation of 3:0-3:1 complexes (Valencia-Gallardo et al., 2022). We hypothesized that IpaA VBS3 induced allosteric changes leads to the exposition of a site in D1D2 responsible for trimerization and that mutations in D2 at residues interfacing IpaA VBS3 should affect trimer formation. To test this, we scrutinized interfacing residues between IpaA VBS3 and D1D2 in the D1D2:IpaA VBS1-3 conformers.

As shown in Fig. 1B, in the close D1D2:IpaA conformer, the IpaA VBS3 helix mostly interacts with the H10 long helix of D2. We could identify a set of putative polar interactions and salt bridges, with IpaA residues T492, E495, K499 and S503 interacting with vinculin residues N393, K139, D389 and K386, respectively (Fig. 1C). In the open conformer, the IpaA VBS3 helix mainly interacts with the H4 long helix of D1, with IpaA residue K499 interacting with vinculin E243. Of note, in this open conformer, an electrostatic clash between vinculin K139 and IpaA K499 may contribute to the dynamics of the IpaA VBS3 during its interaction with different allosteric conformers leading to D1D2 oligomerization (Fig. 1D). All identified vinculin residues were substituted for a charged residue to introduce a charge inversion or disrupt polar interactions using site directed mutagenesis (Materials and Methods, Table 1). We also introduced a mutation at vinculin residue N379 in H10 of D2 that is not expected to establish contact with IpaA VBS3 in the close or open conformer. In this rationale, mutations affecting IpaA VBS3's interface with the close D1D2 conformer are expected to alter its initial docking of IpaA VBS3

on D1D2, whereas the E143K charge inversion would destabilize the open conformer and alter subsequent allosteric changes leading to trimer formation.

Independent of the IpaA VBS3-D1D2 interface, the hidden Markov model-based algorithm MARCOIL predicts the presence of a coiled-coil domain in the same H10 D2 helix between vinculin residues 348 to 393, buried into the D2 helix bundles and adjacent to the IpaA VBS3 interaction sites in the close D1D2 conformer (Fig. S1). This putative coiled-coil domain contains the classical a-g heptad sequence at residues 367-373, with the V367 and A373 corresponding to the "a" and "d" hydrophobic residues, respectively, presumed to intersperse their non-polar side chains at the α-helices interfaces during oligomerization. In our working model, interaction between IpaA VBS3 with D1D2 reveals an oligomerization domain present in D1D2 responsible for trimerization (Valencia-Gallardo et al., 2022), which could involve this putative coiled-coil domain. To test the role of this domain in D1D2 trimerization, we introduced the V367D substitution predicted to disrupt supercoiled helix packing (Fig. S1).

Quantitative analysis of D1D2 trimer formation using CN-PAGE

In previous works, we showed that IpaA induced the formation of D1D2:IpaA 1:1, as well as dimeric complexes and trimeric D1D2 complexes rapidly associating and dissociating an IpaA molecule in SEC-MALS experiments (Valencia-Gallardo et al., 2022). Here, we studied the effets of increasing IpaA molar ratio using SEC and CN(Clear Native)-PAGE. As shown in Fig. 2, at a D1D2:IpaA 1:1 molar ratio, the major peaks with similar amplitude corresponded to the 1:0 and likely the D1D2 trimeric complexes (Fig. 2A, peaks A and C). At a D1D2:IpaA 1:1.5 molar ratio, the D1D2 trimeric complexes represented the major peak (Fig. 2A, peak A). Upon increasing of IpaA molar ratio, a major shifted band (Fig. 2B, A') could also be observed in CN-PAGE followed by Coomassie blue staining, with apo D1D2 rapidly disappearing (Fig. 2B, C') and the formation of intermediate shifted bands (Fig. 2B). The similarity between the distribution of the bands with increasing molar ratio of IpaA in CN-PAGE and the SEC peaks suggested that the A and A' peaks corresponded to trimeric D1D2 complexes. To confirm this, we dissected the A' band form CN-PAGE and analyzed it in a second dimension using regular SDS-PAGE (Materials and Methods) and compared the amounts of D1D2 and IpaA relative to those present in fractions from the SEC peak A. As shown in Fig. 2C, the relative amounts if D1D2 and IpaA were similar for both A and A' samples, with an estimated molar ratio of 3.8

and 3.2, respectively, both values being consistent with a mixture of D1D2:IpaA 3:0 and 3:1 complexes inferred from the SEC-MALS analysis (Valencia-Gallardo et al., 2022).

We used scanning densitometry, to determine the rates of D1D2 trimer formation and D1D2 monomer disappearance normalized to the initial amounts of D1D2 (Materials and Methods). As shown in Fig. 2D, the appearance of D1D2 trimers and disappearance of apo D1D2 as a function of increasing IpaA molar ratio could be nicely adjusted to linear fits with a Pearson coefficient $R^2 > 0.95$. The CN-PAGE assay was used to determine a rate of D1D2 trimer appearance of 1.51 $AU^{-1} \pm 0.3$ (SEM), and D1D2 monomer disappearance of -1.06 $AU^{-1} \pm 0.05$ (SEM) (Table 2).

Characterization of D1D2 mutations affecting trimer formation

We estimated that the CN-PAGE assay was sufficiently robust and reproducible to determine potential differences in rates of trimer formation in the various D1D2 variants. All mutations were introduced in D1D2 and the corresponding variants were purified to homogeneity (Fig. S2). Samples were incubated with increasing molar ratio of the IpaA vinculin-binding domain (aVBD) and analyzed by CN-PAGE followed by Coomassie staining (Materials and Methods). As shown in Figs. 3 and S3, the majority of mutants showed decrease rates of trimer formation (Figs. 3, S3 and Table 2). The rates of D1D2 trimer formation and monomer disappearance were then inferred from linear fits, following quantification by scanning densitometry.

As shown on Table 2, mutations could be distinguished in three types based on to their effects on the rates of D1D2 trimer formation and monomer disappearance. Mutations D389R, E143K and V367D showed delayed rates of D1D2 trimer formation, but no difference in D1D2 monomer disappearance. Mutations K386D, K386G and K139E showed delayed rates of D1D2 trimer formation, as well as increased rates in D1D2 monomer disappearance. The last type of mutations corresponding to N379E and N393D showed no significant effects on trimer formation, but increased rates in monomer disappearance. These results suggest a key role for a knot of polar and charge interactions associated with the D389, K386, and K139 vinculin residues adjacent to IpaA K499 in D1D2 trimerization. Vinculin residue E143 that affects D1D2 trimerization also potentially interacts with IpaA K499 in the open D1D2 conformer. The D389R and E143K charge inversions did not affect monomer disappearance, whereas other

polar mutations with the exception of vinculin V367D targeting the coiled-coil domain led to increase rates of monomer disappearance. While difficult to explain, these results suggest a succession of allosteric interaction between IpaA VBS3 and D1D2 where salt bridges and polar interactions play distinct roles.

Of interest, the mutations in vinculin residues D389R, E143K, K386D, K386G and K139E appear to also show a delay in the decrease of monomer disappearance for aVBD molar ratio inferior to 0.15 relative to that induced in wild-type D1D2 (Figs. 3 and S3), suggesting impairment of initial interaction steps between IpaA and D1D2. The delayed rates of trimer formation associated with V367D also suggest a role for the potential coiled-coil domain. The absence of effects on the rales of D1D2 monomer disappearance for the D389R, E143K and V367D mutations is consistent with the impairment of steps subsequent to the D1D2 1:1 complex formation, involved in D1D2 dimerization or trimerization.

Effects of mutations impairing D1D2 trimerization on focal adhesions

Vinculin oligomerization has been mainly studied in vitro and reported to occur through the Vt-tail domain upon PIP2 stimulation (Thomson et al., 2013). In cells, however, the role of vinculin oligomerization in cell adhesion structures remain unclear. Our studies using a cysteine clamp variant of vinculin deficient for head-domain mediated oligomerization suggest that this property is required for the maturation into large focal adhesions independent of *Shigella* IpaA (Valencia-Gallardo et al., 2022).

To further investigate the role of head domain-mediated vinculin oligomerization in cell adhesions, we transferred mutations altering D1D2 trimerization into full length vinculin fused to mCherry and studied the ability of the vinculin variants to form focal adhesions following transfection in MEF vinculin null cells (Materials and Methods). We studied mutations targeting the knot of polar interactions at the C-terminal extremity of the H10 helix in D2, involved in interaction with IpaA VBS3.

As shown in Fig. 4, cells expressing the D389R, E143 and V367D variants showed a strong spreading defect relative to cells expressing parental mCherrry-vinculin, while no significative difference was observed for the K386D variant (Figs. 4A and 4B). These results correlated with

a strong reduction of focal adhesions in the D389R, E143 and V367D variants with median numbers of FAs ± SD / cell ranging from 45 ± 5 to 64 ± 8, compared to 110 ± 11 for cells expressing parental vinculin (Figs. 4A and 4C). A reduction of the mean number of FAs per cell was also observed for the K386D variant, albeit of lesser amplitude (Figs. 4A and 4C). The decrease in FAs number per cell was also associated with a decrease in their average size in the D389R and E143K variants (Figs. 4A and 4D). We observed no significant decrease in the average FA size for the K386D, consistent with a defect in cell adhesion of lesser amplitude for this latter variant relative to the D389R and E143K variants (Figs. 4A and 4D). Interestingly, the V367D variant also did not show a significant difference in the average FA size compared to control cells expressing parental mCherry-vinculin (Fig. 4D), despite a significant reduction in the number of FAs per cell. The FAs in the V367D variant, although similar in size, looked different than those in control cells, being mostly at the cell periphery and particularly elongated (Fig. 4A). This qualitative difference was confirmed by quantification of the AR index, showing a pronounced difference for the V367D variant compared to the other samples (Fig. 4E).

Discussion

In this work, we identified polar residues located at the C-terminal extremity of the H10 helix in vinculin D2 involved in D1D2 trimerization induced by *Shigella* IpaA. Among mutations reducing IpaA-induced D1D2 trimer formation, we identified the charge inversions at vinculin D389R and E143K that do not affect the rates of monomer disappearance, while the K386D/G polar mutations also led to increased rates of monomer disappearance. IpaA vinculin interaction is mediated by 3 VBSs, IpaA VBS1 and VBS2 interacting with the first and second bundle of D1, respectively. The high affinity of IpaA VBS1-2 to D1 is likely to drive the initial steps leading to the formation of a D1D2: IpaA 1:1 complex, independent of IpaA VBS3. From our modeled structures of the D1D2:IpaA 1:1 complexes, the vinculin D389R and E143K mutations are expected to disfavor IpaA VBS3 binding to the close and open D1D2 conformer, respectively. Hence, the effects of these mutations are in line with specific effects on IpaA VBS3 allosteric changes leading to D1D2 oligomerization without affecting formation of IpaA VBS1, 2-dependent 1:1 D1D2:IpaA complex.

The effects of the K386D/G mutations inversely affecting the rates of D1D2 trimer formation and monomer disappearance are more difficult to explain. There are two possible explanations to explain the increase rates of D1D2 monomer disappearance: i, these polar mutations may increase the rates of IpaA binding to D1D2. This possibility is unlikely because of the predominant role of IpaA VBS1-2 in driving the formation of a D1D2:IpaA 1:1 complex and because these mutations were precisely designed to interfere with IpaA VBS3 interaction with D1D2; ii, they may stabilize an allosteric D1D2 conformer subsequent to the formation of the D1D2:IpaA 1:1 complex, thereby favoring the formation of this latter complex and accelerating monomer disappearance. This possibility is counter-intuitive because it implies that these polar mutations have opposite effects on favoring the formation of an D1D2:IpaA intermediate complex while disfavoring the formation of the trimer. However, it needs to be envisioned since the IpaA VBS3 helix is unlikely to function in the same iterative manner during D1D2 dimerization and resolution into a D1D2 homotrimer, and rather interacts with different subset of residues during these processes. The effects of the K139E mutation also impairing D1D2 trimer formation and accelerating monomer disappearance may be explained in a related yet different manner. Indeed, in apoD1D2, K139 establish a salt bridge with D389 that likely stabilize the D1D2 in the close conformation. The vinculin K139E charge inversion may therefore destabilize D1D2 to favor the formation of intermediate D1D2:IpaA complexes.

We found that the V367D predicted to disrupt the putative CC in D2 H10 affected trimer formation, suggesting a role for this motif in IpaA-induced D1D2 oligomerization. In the structures of apo D1D2 of full-length vinculin, this motif is located at a region of the D2 subdomain exposed on the surface of the vinculin head, but situated at the interface between the D1 and D2 bundle with insufficient space between the subdomains to accommodate another D2 helix bundle for oligomerization. Because the coiled-coil heptad motif is located adjacent to the IpaA VBS3 interaction site with the C-terminal extremity of the H10 helix, one could speculate that IpaA VBS3 binding induces the conformational changes associated with the exposition of this heptad motif. However, this motif remains at the interface of the D1 and D2 subdomains in the open conformer, suggesting that if it plays a role in D1D2 oligomerization, this coiled-coil motif should be exposed in another subsequent intermediate D1D2 conformer.

Our findings based on a clamped-mutant of vinculin proficient for canonical activation but deficient for supra-activation suggest that the head-domain mediated oligomerization of vinculin akin to that induced by IpaA is required for the maturation of adhesions into large focal adhesions (Valencia-Gallardo et al., 2022). The observed effects of the D1D2 mutations support this hypothesis, since the D389R and E143K mutations introduced into full-length vinculin severely affected the number and size of on focal adhesions. While showing reduced and smaller focal adhesions, the amplitude of these defects was less in the K389D vinculin variant. These findings may be related to the different effects of this mutation observed in vitro relative to the D389R and E143K mutations, and to the accumulation of intermediate vinculin oligomeric complexes. Indeed, we previously found that in replating experiments, IpaA favored the rapid adhesion of cell to the substrate, but that similar levels of adhesion were detected over prolonged incubation upon canonical activation including that induced by an IpaA variant deleted for VBS3 (Valencia-Gallardo et al., 2022). The findings suggested that IpaA could promote the supra-activation of vinculin in the absence of mechanotransduction, but that canonical activation associated with mechanotransduction could also induce supra-activation. It is possible that the accumulation of oligomeric complexes linked to the K386D mutation compensate the defect of IpaA-induced trimers, during mechanotransduction.

The size reduction of focal adhesions in D1D2 mutants was more specifically observed at the levels of peripheral adhesions, while little difference was observed for ventral adhesions relative to parental vinculin. These ventral adhesions appeared thin and elongated, consistent with fibrillar adhesions known to remain stable independent of force (Sun et al., 2016). These observations are consistent with head domain-mediated vinculin oligomerization occurring at high force regime. As opposed to other mutations, the V367D mutation led to a drastic reduction of the number of focal adhesions but did not affect their average size. Instead, the V367D variant mostly formed elongated adhesions at the cell periphery. While the role of the putative coiled-coil domain targeted by the V367D mutation deserves clarification, the effects on the focal adhesion morphology associated with this particular mutation is consistent with the impairment in a process during vinculin oligomerization and focal adhesion formation that is different than the other mutations.

Materials and Methods

Bacterial strains, cells and plasmids

The bacterial strain used for the purification of D1D2 construct is *E. coli* BL21 (DE3) from Invitrogen. *E. coli* DH5-α F– *endA1 glnV44 thi-1 recA1 relA1 gyrA96 deoR nupG purB20 φ80dlacZΔM15 Δ(lacZYA-argF) U169, hsdR17(rK–mK+), λ– was* used for the purification of aVBD. MEF and MEF vinculin null cells (Humphries, Wang et al. 2007) were grown in DMEM 1 g / L glucose containing 10 % FCS in a 37°C incubator containing 10 % CO_2.

The pGEX4T2-AVBS1-3 encoding aVBD and the pET15b-D1D2 plasmids were described previously. The mutations in D1D2 were introduced by site-directed mutagenesis using pET15b-D1D2 as a matrix and the primer pairs indicated in Table 1. The pmCherry-human vinculin (HV) and was from Addgene. Mutations in D1D2 were transferred in mCherry-HV by exchanging the NheI-PspXI fragment with the corresponding XbaI-PspXI fragment of pET15b-D1D2.

Protein purification

BL21 (DE3) competent *E. coli* was transformed with the pET15b-D1D2 variant constructs. D1D2 were purified as described (Park, Valencia-Gallardo et al. 2011). For the IpaA derivatives, DH5-a competent *E. coli* was transformed with pGEX-4T2-AVBS1-3. Bacteria were grown at 37°C with shaking until OD_{600nm} = 1.0 were induced with 1 mM IPTG and incubated for another 2 hrs. Bacteria were pelleted and washed in ice-cold lysis buffer containing 25 mM Tris PH 7.4, 100 mM NaCl and 1 mM beta-mercaptoethanol, containing Complete™ protease inhibitor. All subsequent steps were performed at 4°C. Bacterial pellets were resuspended in 1/20th of the original culture volume and lyzed using a microfluidizer (LM20, Microfluidics). Cell debris were pelleted by centrifugation at 8000 xg for 20 min. Clarified lysates were subjected to affinity chromatography using a GSTrap HP affinity column (GE Healthcare). Briefly, following incubation with the clarified lysates, the column was washed with five column volumes prior to incubation in PBS containing 100 μg / ml Thrombin (Cytiva, ref 27084601) for 16 hours at 21°C. aVBD was then eluted in PBS and further subjected to purification using size exclusion chromatography using a Superdex 200 10/300 GL (Ge Healthcare). Samples were stored aliquoted at -80°C at concentrations ranging from 1 to 10 mg/ml.

SEC analysis

D1D2 and aVBD were at the indicated molar ratio, with D1D2 at a final concentration of 20 μM, for 60 minutes at 21°C. 200µl of the protein mixtures were analyzed by size-exclusion chromatography (SEC) on a Superdex 200 10/300 GL (GE Healthcare) using a GE ÄKTA FPLC™ (Fast Protein Liquid Chromatograph, GMI) and a collection volume of 200 µl per fraction and 20ml of total collected volume. The SEC buffer was 25 mM Tris-HCl pH 7.2, 100 mM NaCl.

.

CN-PAGE

The D1D2 variants and aVBD were at the indicated molar ratio, with D1D2 at a final concentration of 20 μM, for 60 minutes at 21°C. Protein complex formation was visualized by PAGE under non-denaturing conditions using à 7.5% polycrylamide gel, followed by Coomassie blue staining, as described previously (ref).

Cell transfection

For transfection experiments, cells were seeded at 1 x 10^4 cells on 25 mm-diameter coverslips coated with fibronectin at a concentration of 20 μg / ml. Cells were transfected with 1 µg of the pGEX-4T2-D1D2 construct and 4 µls JetPEI transfection reagent (Polyplus) for 16 hours following the manufacturer's recommendations.

Fluorescence confocal microscopy analysis

Samples were fixed in PBS containing 3.7 % paraformaldehyde for 60 min at 21°C, prior to processing for fluorescence staining of F-actin using Phalloidin-Alexa 488 as previously described (Valencia-Gallardo et al., 2022). Samples were analyzed using an Eclipse Ti inverted microscope (Nikon) equipped with a 60 x objective APO TIRF oil immersion (NA: 1.49), a CSU-X1 spinning disk confocal head (Yokogawa), and a Prime 95B sCMOS camera (Photometrics) controlled by the Metamorph 7.7 software.

Image analysis

Focal adhesions were analyzed using the ImageJ 2.1.0/1.53c software. For each set of experiments, the confocal plane corresponding to the basal plane was subjected to thresholding using strictly identical parameters between samples. Adhesion clusters were detected using the "Analyze particle" plug-in, setting a minimal size of 3.5 μm^2.

Statistical analysis

The number of adhesions was analyzed using Dunn's multiple comparisons test. The median area was compared using Mann-Whitney test. Differences in the rates of D1D2 trimer formation and monomer disappearance based were analyzed using an ANCOVA test.

Acknowledgements

The research was supported by fundings from the Inserm and CNRS. GTVN is a recipient of the grant ANR-21-CE35-0007-03 CALPLYCX. DA and BCC received funding from the CONACYT. HK received a grant from the Swiss National Science Foundation (grant no. SNF P2ZHP3_191289).

References

1. Bays JL, DeMali KA. Vinculin in cell-cell and cell-matrix adhesions. Cell Mol Life Sci. 2017 Aug;74(16):2999-3009. doi: 10.1007/s00018-017-2511-3. Epub 2017 Apr 11. PMID: 28401269; PMCID: PMC5501900.
2. Goldmann WH. Role of vinculin in cellular mechanotransduction. Cell Biol Int. 2016 Mar;40(3):241-56.
3. Peng X, Nelson ES, Maiers JL, DeMali KA. New insights into vinculin function and regulation. Int Rev Cell Mol Biol. 2011;287:191-231.
4. Atherton P, Stutchbury B, Jethwa D, Ballestrem C. Mechanosensitive components of integrin adhesions: Role of vinculin. Exp Cell Res. 2016 Apr 10;343(1):21-27.
5. Parsons JT, Horwitz AR, Schwartz MA. Cell adhesion: integrating cytoskeletal dynamics and cellular tension. Nat Rev Mol Cell Biol. 2010 Sep;11(9):633-43.
6. Yan J, Yao M, Goult BT, Sheetz MP. Talin Dependent Mechanosensitivity of Cell Focal Adhesions. Cell Mol Bioeng. 2015;8(1):151-159.
7. Kluger C, Braun L, Sedlak SM, Pippig DA, Bauer MS, Miller K, Milles LF, Gaub HE, Vogel V. Different Vinculin Binding Sites Use the Same Mechanism to Regulate Directional Force Transduction. Biophys J. 2020 Mar 24;118(6):1344-1356.
8. Gingras AR, Ziegler WH, Frank R, Barsukov IL, Roberts GC, Critchley DR, Emsley J. Mapping and consensus sequence identification for multiple vinculin binding sites within the talin rod. J Biol Chem. 2005 Nov 4;280(44):37217-24.
9. Izard T, Evans G, Borgon RA, Rush CL, Bricogne G, Bois PR. Vinculin activation by talin through helical bundle conversion. Nature. 2004 Jan 8;427(6970):171-5.
10. Sun Z, Guo SS, Fässler R. Integrin-mediated mechanotransduction. J Cell Biol. 2016 Nov 21;215(4):445-456.

11. Goult BT, Brown NH, Schwartz MA. Talin in mechanotransduction and mechanomemory at a glance. J Cell Sci. 2021 Oct 15;134(20):jcs258749.
12. Yao M, Goult BT, Klapholz B, Hu X, Toseland CP, Guo Y, Cong P, Sheetz MP, Yan J. The mechanical response of talin. Nat Commun. 2016 Jul 7;7:11966. doi: 10.1038/ncomms11966.
13. Izard T, Brown DT. Mechanisms and Functions of Vinculin Interactions with Phospholipids at Cell Adhesion Sites. J Biol Chem. 2016 Feb 5;291(6):2548-55.
14. Auernheimer V, Lautscham LA, Leidenberger M, Friedrich O, Kappes B, Fabry B, Goldmann WH. Vinculin phosphorylation at residues Y100 and Y1065 is required for cellular force transmission. J Cell Sci. 2015 Sep 15;128(18):3435-43.
15. Thwaites TR, Pedrosa AT, Peacock TP, Carabeo RA. Vinculin Interacts with the Chlamydia Effector TarP Via a Tripartite Vinculin Binding Domain to Mediate Actin Recruitment and Assembly at the Plasma Membrane. Front Cell Infect Microbiol. 2015 Nov 30;5:88.
16. Park H, Lee JH, Gouin E, Cossart P, Izard T. The rickettsia surface cell antigen 4 applies mimicry to bind to and activate vinculin. J Biol Chem. 2011 Oct 7;286(40):35096-103.
17. Valencia-Gallardo CM, Carayol N, Tran Van Nhieu G. Cytoskeletal mechanics during Shigella invasion and dissemination in epithelial cells. Cell Microbiol. 2015 Feb;17(2):174-82.
18. Izard T, Tran Van Nhieu G, Bois PR. Shigella applies molecular mimicry to subvert vinculin and invade host cells. J Cell Biol. 2006 Nov 6;175(3):465-75.
19. Tran Van Nhieu G, Izard T. Vinculin binding in its closed conformation by a helix addition mechanism. EMBO J. 2007 Oct 31;26(21):4588-96. doi: 10.1038/sj.emboj.7601863. Epub 2007 Oct 11. Erratum in: EMBO J. 2008 Mar 19;27(6):922.
20. Park H, Valencia-Gallardo C, Sharff A, Tran Van Nhieu G, Izard T. Novel vinculin binding site of the IpaA invasin of Shigella. J Biol Chem. 2011 Jul 1;286(26):23214-21.
21. Valencia-Gallardo C, Bou-Nader C, Aguilar-Salvador DI, Carayol N, Quenech'Du N, Pecqueur L, Park H, Fontecave M, Izard T, Tran Van Nhieu G. Shigella IpaA Binding to Talin Stimulates Filopodial Capture and Cell Adhesion. Cell Rep. 2019 Jan 22;26(4):921-932.
22. Valencia-Gallardo C, Aguilar-Salvador D, Khakzad H, Cocom-Chan B, Bou-Nader C, Velours C, Zarrouk Y, Le Clainche C, Malosse C, Borges Lima D, Quenech'Du N, Mazhar B, Essid S, Fontecave M, Asnacios A, Chamot-Rooke J, Malmström L, Tran Van Nhieu G. BioRXive. doi: http://doi.org/10.1101/2 022.11.07.515412.
23. Molony L, Burridge K. Molecular shape and self-association of vinculin and metavinculin. J Cell Biochem. 1985;29(1):31-6.
24. Bakolitsa C, de Pereda JM, Bagshaw CR, Critchley DR, Liddington RC. Crystal structure of the vinculin tail suggests a pathway for activation. Cell. 1999 Dec 10;99(6):603-13. doi: 10.1016/s0092-8674(00)81549-4. PMID: 10612396.

25. Chinthalapudi K, Rangarajan ES, Patil DN, George EM, Brown DT, Izard T. Lipid binding promotes oligomerization and focal adhesion activity of vinculin. J Cell Biol. 2014 Dec 8;207(5):643-56.
26. Johnson RP, Craig SW. Actin activates a cryptic dimerization potential of the vinculin tail domain. J Biol Chem. 2000 Jan 7;275(1):95-105.
27. Huang DL, Bax NA, Buckley CD, Weis WI, Dunn AR. Vinculin forms a directionally asymmetric catch bond with F-actin. Science. 2017 Aug 18;357(6352):703-706.
28. Thompson PM, Tolbert CE, Campbell SL. Vinculin and metavinculin: oligomerization and interactions with F-actin. FEBS Lett. 2013 Apr 17;587(8):1220-9.
29. Garakani K, Shams H, Mofrad MRK. Mechanosensitive Conformation of Vinculin Regulates Its Binding to MAPK1. Biophys J. 2017 May 9;112(9):1885-1893.

Figure and legends

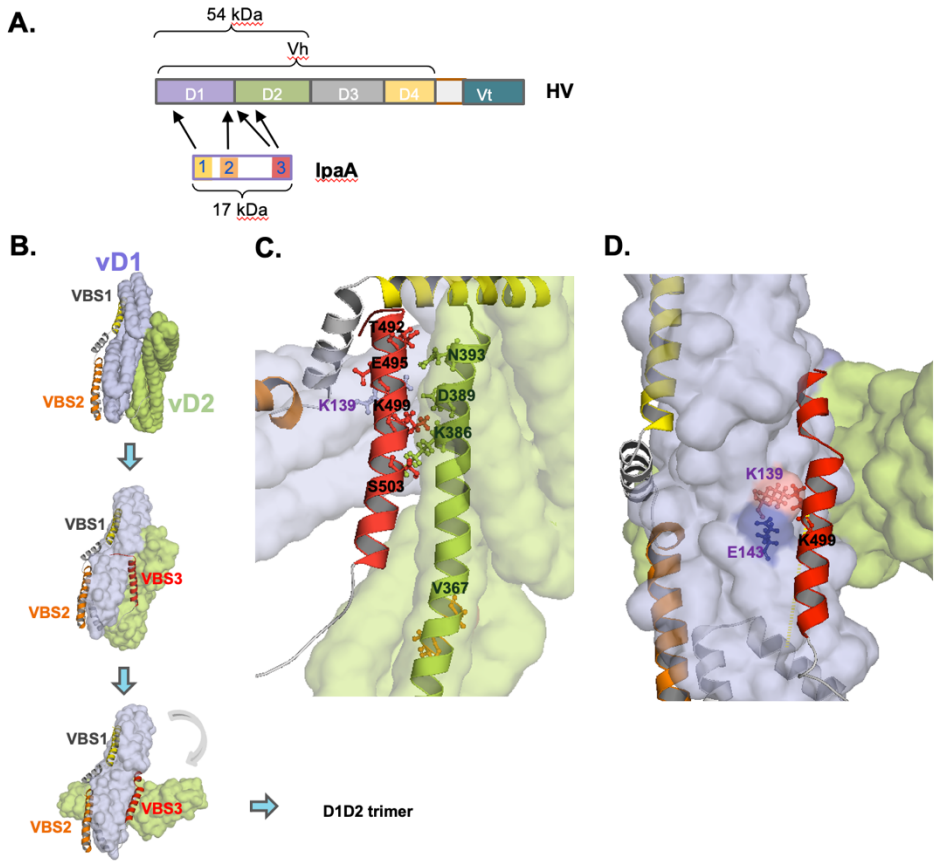

Fig. 1 Design of D1D2 mutations targeting IpaA VBS3 contact sites

A, Schematic organization of vinculin subdomains and IpaA vinculin-binding domain. The molecular weight of the vinculin D1D2 and IpaA vinculin-binding domains is indicated. The arrows point at binding of: IpaA VBS1 to the D1 first bundle, IpaA VBS2 to the second D1 bundle, IpaA VBs3 binding to the D1D2 interface and D2 second bundle. **B-D**, TX-MS based models of D1D2: aVBD. The vinculin D1 and D2 are shown as grey and green surface structures, respectively. IpaA VBSs are shown as ribbon structures. **B**, Top: IpaA VBS1-2 binds to a D1D2 that adopts a conformation similar to that of apoD1D2 (close conformer). Concomitant binding of IpaA VBS3 to the D2 first bundle leads to a similar D1D2 conformation (Middle, while binding of IpA VBS3 to the D1D2 interface induces a major conformational change (open conformer) with a 30° tilt in the relative orientation of the D1 and D2 major axis. **C, D**, higher magnifications showing the IpaA VBS3(red) interface with D1 D2 in the close (**C**) and open (**D**) conformer. The residues potentially involved in polar interactions via their side chains are indicated. In the open conformer, IpaA K499 may interact with E143 or clash with K139 on vinculin D1.

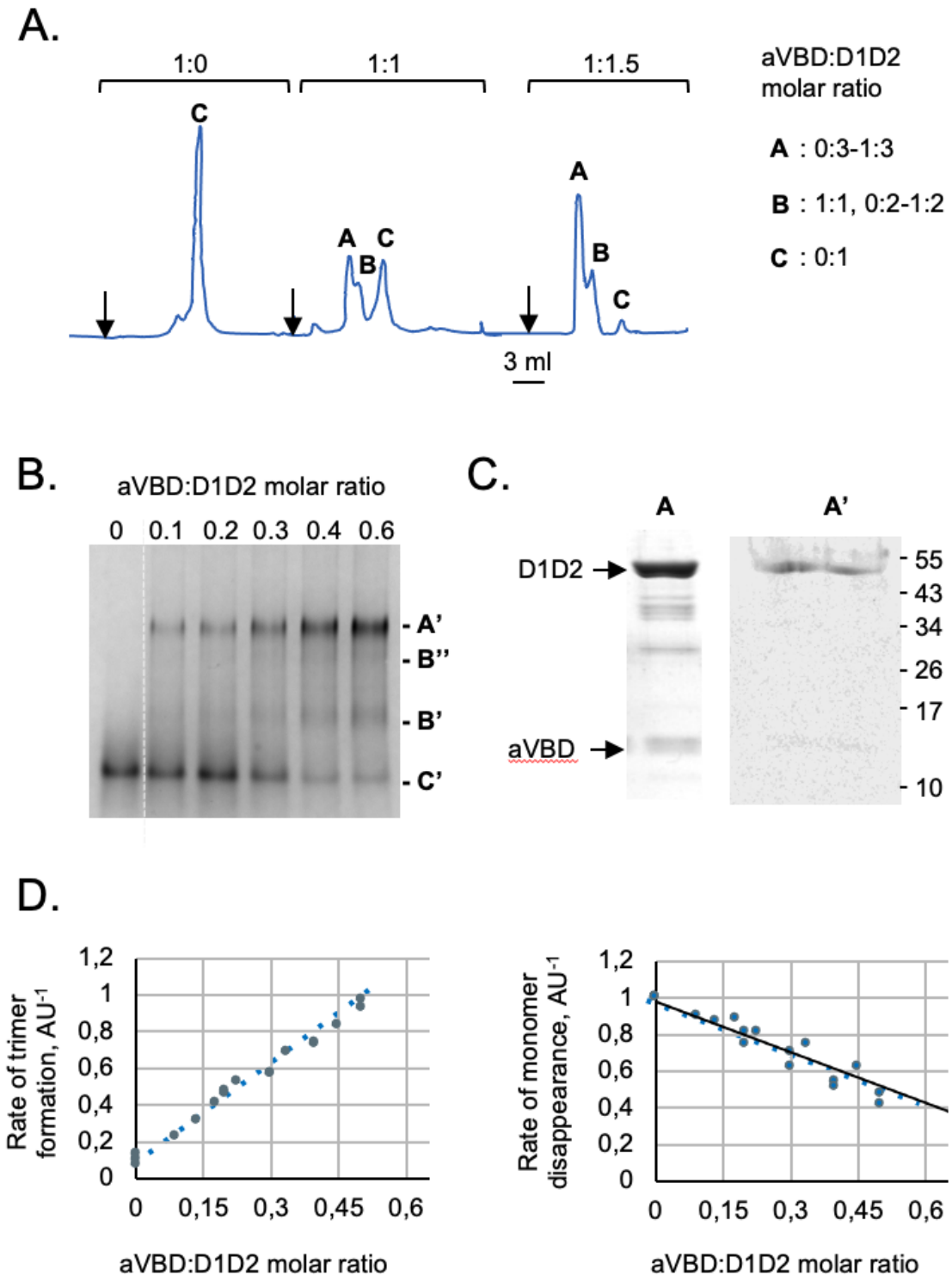

Fig. 2. A CN-PAGE assay to study IpaA-induced D1D2 trimer formation

A, **B**. aVBD and D1D2 were mixed at the indicated molar ratio, with D1D2 at a final concentration of 20 µM, and incubated for 60 min at 21°C prior to analysis. **A**, SEC analysis using an Increase Superdex 200 (Materials and Methods). The indicated stoichiometry is inferred from previous SEC-MALS analysis (ref) molecular and the mass of complexes in peaks

A, B and C estimated from molecular weight standards as a function of the respective elution volume. **B**, CN-PAGE using a 10 % polyacrylamide native gel followed by Coomassie blue staining. C': monomeric D1D2.4, B' and B": aVBD:D1D2 complexes. **C**, SDS-PAGE followed by Coomassie blue staining of samples corresponding to peak A in SEC fractionation as shown in panel A (A) and eluted following dissection of band A' as shown in Panel D (A'). Densitometry analysis of the bands indicated a D1D2:aVBD ratio of 3.8 and 3.2 for sample A and A', respectively, consistent with 3:0-3:1 aVBD complexes. **D**, the integrated intensity of bands corresponding to trimeric (A') or monomeric D1D2 (C) were scanned by densitometry, and normalized to that of monomeric D1D2 in the absence of aVBD. The graphs are representative of at least three independent experiments.

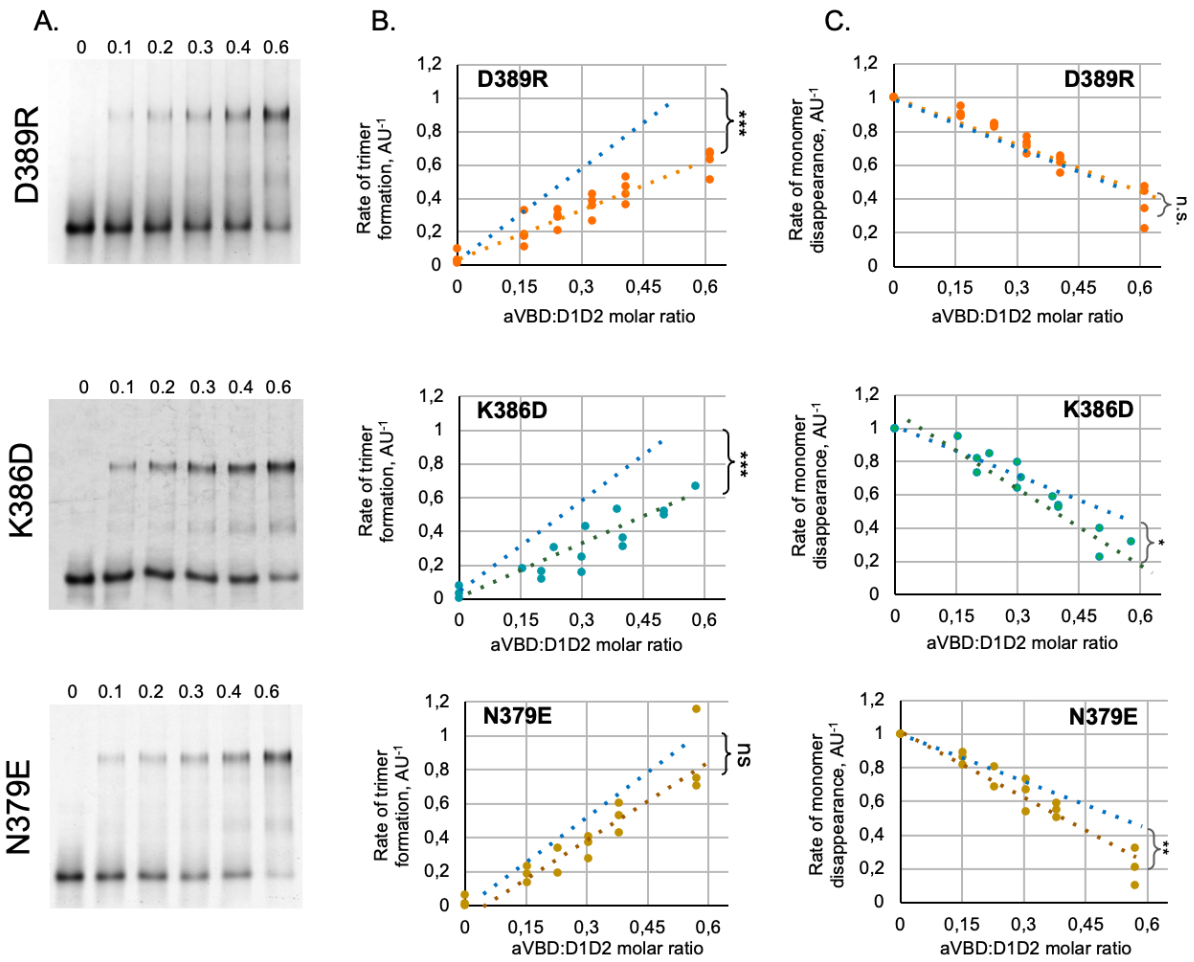

Fig. 3. Effects of mutations on D1D2 trimer formation and monomer disappearance.

A, CN-PAGE using a 10 % polyacrylamide native gel followed by Coomassie blue staining of aVBD-induced complex formation with the indicated D1D2 variant. The aVBD:D1D2 molar ratio is indicated above each lane. **B**, **C**, the integrated intensity of bands corresponding to

trimeric (**B**) or monomeric D1D2 (**C**) were scanned by densitometry, and normalized to that of monomeric D1D2 in the absence of aVBD. The graphs are representative of at least three independent experiments. The blue dashed lines correspond to linear fits obtained for parental D1D2. ANCOVA test: *: $p < 0.05$; **: $p < 0.01$; ***: $p < 0.005$. ns: not significant.

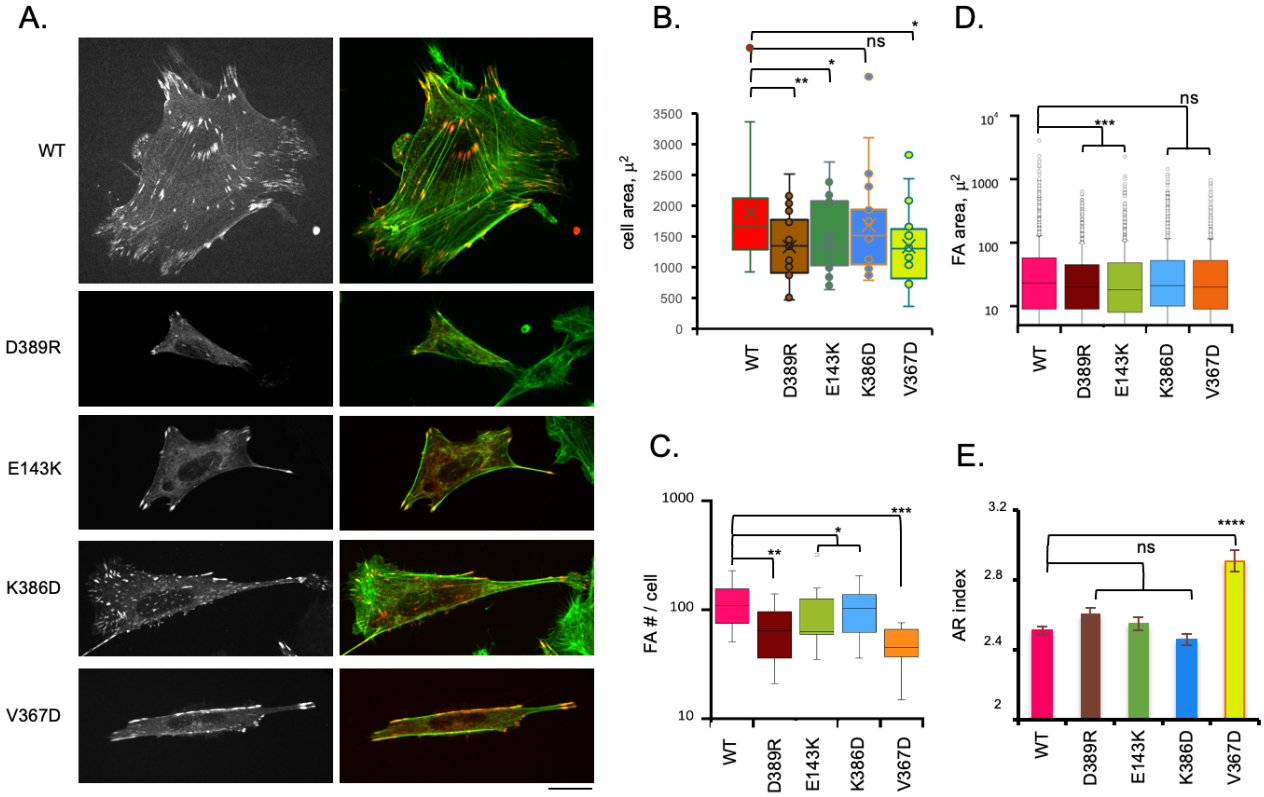

Fig. 4. Effects of D1D2 mutations affecting D1D2 trimer formation on focal adhesions

MEF vinculin -/- cells were transfected with HV-mCherry variants bearing the indicated mutation. Samples were fixed and processed for fluorescence staining of F-actin. **A**, Left panels: HV mCherry. Right panels: green: F-actin; red:HV mCherry. B, cell spreading area. C, average number of FAs per cell (n > 20, N = 2); D, average FA size; E: AR index corresponding to the major over minor axis of FA. C-E, (n > 2500, N = 2). Mann-Whitney: *: $p < 0.05$; **: $p < 0.01$; ***: $p < 0.005$. ns: not significant.

D1D2 mutation	primers
D389R	5'-CATTGCAAAGAAGATCCGTGCTGCTCAGAACTGGC-3' 5'- GCCAGTTCTGAGCAGCACGGATCTTCTTTGCAATG-3'
E143K	5'- AGGAATTTTGaaaTATCTTACAGTG -3' 5'- CACTGTAAGATAtttCAAAATTCCT-3'
K386D	5'- GAGCATTGCAgacAAGATCGATGC-3' 5'- GCATCGATCTTgtcTGCAATGCTC-3'
K386G	5'- CAAAGCAGAGCATTGCAGGCAAGATCGATGCTGCTC -3' 5'- GAGCAGCATCGATCTTGCCTGCAATGCTCTGCTTTG-3'
K139E	5'- TAGAGTTTGCgaaGGAATTTTGG-3' 5'-CCAAAATTCCttcGCAAACTCTA-3'
V367D	5'-CTCACAGCAAAAGTGGAAAATGCAGCTCGC-3' 5'-GCGAGCTGCATTTTCCACTTTTGCTGTGAG -3'
N393D	5'-GATCGATGCTGCTCAGGACTGGCTTGCAGATCCAAATG-3' 5'-CATTTGGATCTGCAAGCCAGTCCTGAGCAGCATCGATC-3'
N379E	5'- GCTGGAAGCCATGACCGAATCAAAGCAGAGCATTGC -3' 5'- GCAATGCTCTGCTTTGATTCGGTCATGGCTTCCAGC-3'

Table 1. Primers used in this study.

D1D2 construct	Rate of trimer formation AU^{-1}	Rate of Monomer Disappearance AU^{-1}
WT	1.51 ± 0.03	-1.06 ± 0.05
D389R	0.95 ± 0.06 ***	-1.06 ± 0.05 n.s.
E143K	1.10 ± 0.068 ***	-0.88 ± 0.10 n.s.
V367D	1.19 ± 0.04 ***	-0.88 ± 0.11 n.s.
K386D	0.99 ± 0.099 ***	-1.29 ± 0.059 *
K386G	1.12 ± 0.04 **	-1.39 ± 0.06 *
K139E	1.04 ± 0.08 ***	-1.42 ± 0.069 *
N393D	1.30 ± 0.05 n.s.	-1.32 ± 0.04*
N379E	1.48 ± 0.059 n.s.	-1.38 ± 0.04 **

Table 2. Rates of D1D2 trimer formation and monomer disappearance.

The rates of trimer formation and monomer disappearance for the indicated D1D2 variants were inferred from linear fits (Materials and Methods). ANCOVA test: *: $p < 0.05$; **: $p < 0.01$; ***: $p < 0.005$. ns: not significant.

: and;

: and; E143K: 5’- -3’ and 5’- -3’; E143K: 5’- -3’ and 5’- -3’;

Acknowledgements

Supplementary Materials

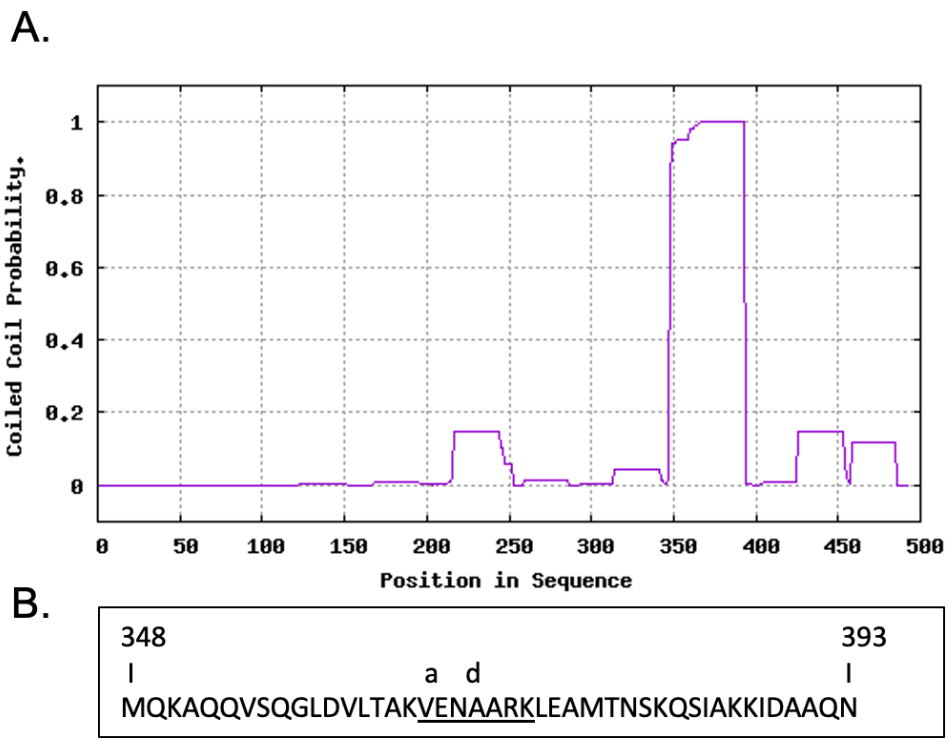

Fig. S1. Predicted coiled-coil motif in D2
A, the coiled-coil probability in D1D2 corresponding to vinculin residues 1-484 assessed using the MARCOIL algorithm with threshold 50: 11 (ref), identified a coiled-coil region between residues 348-393 with max = 99.9. **B**, sequence of the predicted coiled-coil region identified in A. The numbers correspond to the residue numbers in the vinculin sequence. The canonical heptad region is underlined, with a and d corresponding to hydrophobic residues at position V367 and A370, respectively. The V367D mutation is predicted to abolish coiled-coil formation.

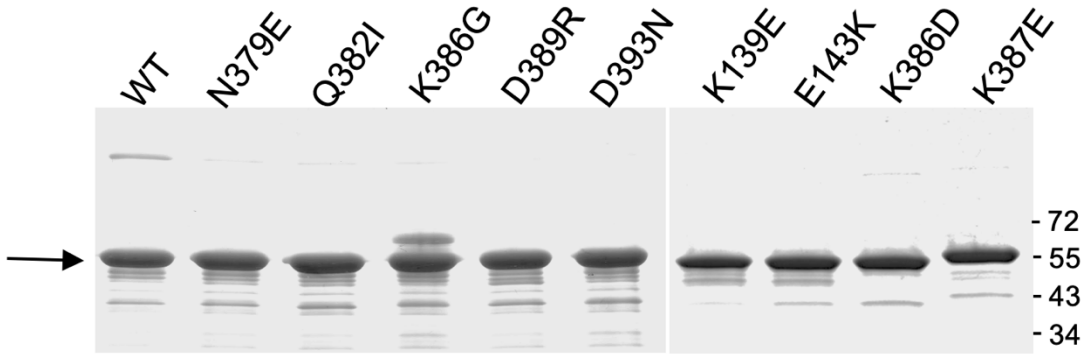

Fig. S2. SDS-PAGE purified D1D2 variants

D1D2 variants expressed in E. coli BL21 (DE3) and purified by affinity chromatography (Materials and Methods) were analyzed by SDS-PAGE using a 10 % polyacrylamide gel followed by Coomassie staining. The size of the molecular weight markers is indicated in kDa. The arrow points at D1D2 constructs.

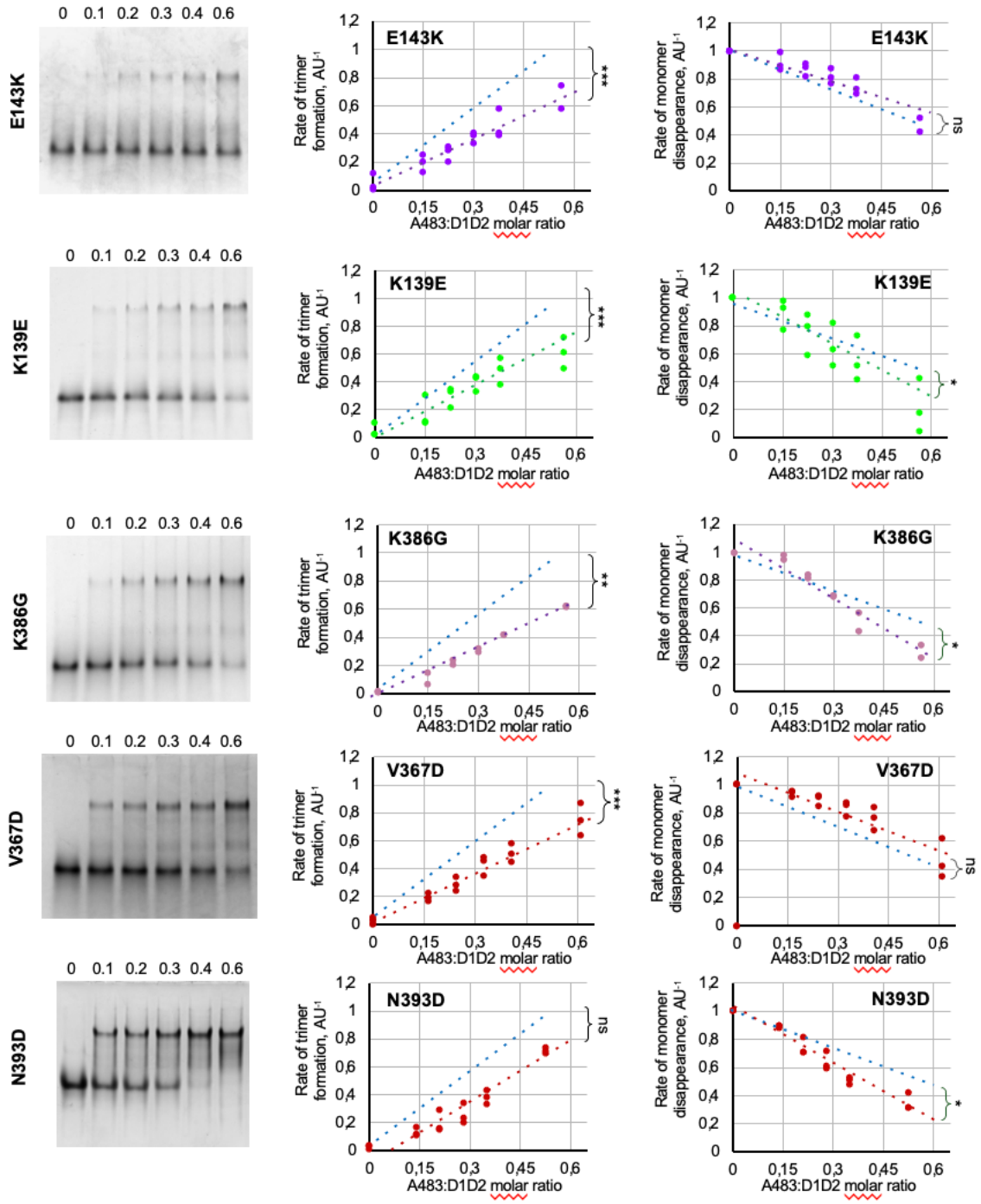

Fig. S3. Effects of D1D2 mutations on IpaA-induced trimer formation and monomer disappearance.

Left panels, CN-PAGE using a 10 % polyacrylamide native gel followed by Coomassie blue staining of aVBD-induced complex formation with the indicated D1D2 variant. The aVBD:D1D2 molar ratio is indicated above each lane**. Center and right panels**, the integrated intensity of bands corresponding to trimeric (**center**) or monomeric D1D2 (**right**) were scanned by densitometry, and normalized to that of monomeric D1D2 in the absence of aVBD. The graphs

are representative of at least three independent experiments. The blue dashed lines correspond to linear fits obtained for parental D1D2. ANCOVA test: *: $p < 0.05$; **: $p < 0.01$; ***: $p < 0.005$. ns: not significant.